Anion exchange membranes composed of poly(*m*-terphenylene)s and pendant ammonium head groups for anion exchange membrane water electrolyzers

Vikrant Yadav,[a] Kenji Miyatake[a,b,c,*] Fanghua Liu,[a] Fang Xian,[a] Ahmed Mohamed Ahmed Mahmoud,[a,d] Katsuyoshi Kakinuma,[a,b] Toshio Iwataki,[b] and Makoto Uchida[b]

[a] Clean Energy Research Center, University of Yamanashi, Kofu, 400-8510, Japan

[b] Hydrogen and Fuel Cell Nanomaterials Center, University of Yamanashi, 4 Takeda, Kofu, Yamanashi 400-8510, Japan

[c] Department of Applied Chemistry, Waseda University, Tokyo 169-8555, Japan

[d]Office of Institutional Advancement and Communications, Kyoto University, Kyoto 606851, Japan.

*Corresponding author

E-mail address: miyatake@yamanashi.ac.jp (K. Miyatake)

Materials

1,3-Bis(2-(4-aminophenyl)-2-propyl)benzene (>98.0%), fluorene (>95.0%), 1,6-dibromohexane (>97.0%), N-chlorosuccinimide (NCS) (>98.0%), Copper(I) chloride (>95.0%), and tetrabutylammonium bromide (TBAB) (>99.0%) were obtained from TCI, Japan and used as received. Sodium nitrite (>97.0%), bis(1,5-cyclooctadiene)nickel(0) ($Ni(COD)_2$) (>95.0%), N,N-dimethylacetamide (DMAc) (>99%), dimethyl sulfate (extra pure), dimethyl sulfoxide-d_6 (DMSO-d_6) with 0.03% tetramethylsilane (TMS) (100 atom% D), chloroform-*d* ($CDCl_3$) with 0.03% TMS (100 atom% D) were purchased from Kanto Chemicals, Japan and used as received. Other chemicals were of commercially available grade and used as received. For the copolymerization reaction, N, N-dimethylacetamide (DMAc) was purified using a solvent refining apparatus.

Synthesis of monomers

Synthesis of 1,3-bis(2-(4-chlorophenyl)propenyl)benzene (*m*T) is as follows (Scheme S1). 1,3-Bis(2-(4-aminophenyl)-2-propyl)benzene (15.00 g, 43.54 mmol) was dispersed in 150 mL of 8M aq. HCl at r.t. in a conical flask, and then the flask was placed in an ice bath. To the dispersion was added 37 mL of $NaNO_2$ (12.19 g, 174.16 mmol) aq. dropwise at 0-5 ^oC, and stirring was continued for 15 min at the same temperature. To the resultant solution, CuCl (21.55 g, 217.70 mmol) in 86 mL of conc. HCl was added dropwise, and the reaction was allowed for 12 h at r.t. The solution was neutralized using 2.5M K_2CO_3 aq., and the aqueous layer was extracted with ethyl acetate. The organic layer was washed with water, dried over Na_2SO_4, and concentrated under reduced pressure. The resultant crude liquid was purified by silica gel chromatography (eluent: hexane) to afford the target *m*T monomer in 42% yield (7.04 g) as a white crystalline solid. 6,6'-(2,7-Dichloro-

9H-fluorene-9,9-diyl)bis(*N,N*-dimethylhexan-1-amine) (AF) was synthesized following our previous report in 83% yield as a light yellow crystalline solid.[1]

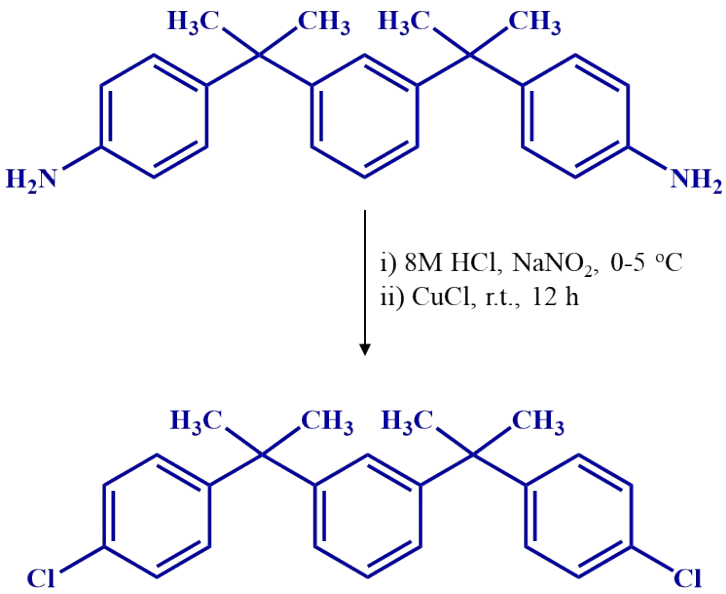

Scheme S1. Synthesis of 1,3-bis(2-(4-chlorophenyl)propenyl)benzene.

Membranes fabrication and ion exchange reactions

A 3.0 wt.% quaternized copolymer solution in DMAc was prepared at 50 °C, filtered through a 0.45-μm membrane filter, degassed, and cast onto a glass plate. Transparent membranes were obtained after 24 hours of drying at 50 °C with a thickness of 45 ± 5 μm. As-obtained membranes were ion-exchanged to OH^- using 1M KOH at 80 °C for 24 hours, then further exchanged in 1M HCl or 0.1M K_2PtCl_4 at 40 °C for 48 hours to obtain Cl^- or $PtCl_4^{2-}$ forms, respectively.

Measurements

^1H NMR spectra were recorded on a JEOL JNM-ECA/ECX500 spectrometer using

$CDCl_3$ or DMSO-d_6 with TMS as an internal reference.

The molecular weight of precursor copolymers was determined by gel permeation chromatography (GPC) with a Shodex K-805 L column and a Jasco UV 2077 detector (270 nm), using $CHCl_3$ with 0.03M triethylamine as the eluent, calibrated with polystyrene standards (M_n = 1.26 to 423 kDa).

Dry $PtCl_4^{2-}$-form membranes were embedded in epoxy resin, sectioned to 50 nm with a Leica microtome Ultracut UCT, and mounted on a copper grid. TEM images were obtained using a Hitachi H-9500 microscope at 200 kV.

Humidity-dependent small-angle X-ray scattering (SAXS) profiles for Cl^--form membranes were measured at 40 °C on a Rigaku Nano Viewer with Cu(Kα) X-rays, with samples equilibrated for 2 hours at each humidity condition.

Ion exchange capacity, water uptake, and swelling ratio

IEC values were estimated by the Mohr's titration method. Dried membrane samples (ca. 20 in Cl^- form) were ion-exchanged by immersion in 0.2M aq. $NaNO_3$ solution for 24 h at r.t., and the solution containing released Cl^- ions was titrated with 0.01M aq. $AgNO_3$ solution, where 0.25M aq. K_2CrO_4 and 0.10M aq. $NaHCO_3$ solutions were the indicator and pH adjuster, respectively. Titrated IEC values were calculated using the following equation:

$$IEC_{tit}\ (\text{meq. g}^{-1}) = \frac{V \times C}{W_{dry}}$$

where, V and C are the titer volume and concentration of $AgNO_3$.

Water uptake and swelling ratio were measured in liquid water at 30 °C using the following equation:

$$\text{Water uptake} = \frac{W_{wet} - W_{dry}}{W_{dry}} \times 100\ (\%)$$

$$\text{Swelling ratio}\ (\%) = \frac{T_{wet} - T_{dry}}{T_{dry}} \times 100\ (\%)$$

Hydroxide ion conductivity and hydroxide ion diffusion coefficient

Hydroxide conductivity was measured at temperatures ranging from 30 to 80 °C (at 10 °C increments) in degassed, deionized water (18 MΩ) under a nitrogen atmosphere. Impedance was recorded using a four-probe AC impedance analyzer (Solartron 1255B) over a frequency range of 0.001 to 100 kHz. Conductivity was calculated from the membrane's cross-sectional area (A, cm^2), the distance between reference electrodes (L, cm), and the measured resistance (R, Ω) at each temperature using the following equation:

$$\sigma\ (S\ cm^{-1}) = \frac{L}{(R \times A)}$$

The Nernst-Einstein equation was used to calculate the hydroxide ion diffusion coefficient:

$$D_\sigma = \frac{\sigma \times R \times T}{IEC_{vol} \times F^2}$$

where σ is the measured hydroxide ion conductivity at 30 °C, R is the gas constant (8.314 J K^{-1} mol^{-1}), T is the absolute temperature (303.15 K), IEC_{vol} is the volumetric ion exchange capacity (mmol cm^{-3}; moles of ammonium groups per unit volume of wet membrane), and F is the Faraday constant (96485 C mol^{-1}).

Measurements for ion exchange capacity, water uptake, swelling ratio, and hydroxide ion

conductivity were performed in triplicate, and the results were averaged.

Viscoelastic and mechanical properties

Dynamic mechanical analysis (DMA) of Cl^--ion exchanged membrane samples was performed using an ITK DVA-225 viscoelastic analyzer. Viscoelastic properties (storage modulus, loss modulus, and tan δ) were measured from 30 to 90 °C at a heating rate of 1°C min^-, 60% relative humidity (RH), and 10 Hz frequency. Humidity dependence was tested from 0 to 90% RH at 80 °C and 10 Hz.

Stress-strain behavior of dumbbell shape (2 × 10 mm) membrane samples (Cl^- form) was evaluated at 80 °C and 60% RH using a universal testing machine (UTM Autograph AGS-J500N) with a temperature and humidity-controlled chamber. Preconditioned (3 h) membrane samples were tested at a 10 mm min^{-1} stretching rate, with three measurements per sample.

Alkaline stability

Alkaline stability was assessed by immersing membranes in 8M KOH at 80 °C for 1,000 hours. Hydroxide ion conductivity was measured periodically, with solution replacement every 200 hours. Post-test analysis includes IEC measurement and ^1H NMR (in Cl^- form) analysis.

Membrane-electrode assembly preparation

A membrane-electrode assembly (MEA) was fabricated following a procedure adapted from our previous work.[2] To prepare the anode catalyst ink, an in-house synthesized

$Ni_{0.8}Fe_{0.2}O$[3] catalyst was dispersed with QPAF-4[1] ionomer (5 wt.% in methanol; IEC = 1.50 meq g^{-1}) and ultrapure water. The ionomer-to-catalyst mass was set at 0.15. This ink was applied onto one side of a *m*T-QAF membrane (17 μm thickness) using a Nordson pulse-swirl-spray (PSS) system to produce a catalyst-coated membrane (CCM) with a geometric active area of 1.0 cm^2. The anode catalyst loading was 2.36 mg cm^{-2}. A nickel porous transport layer (PTL; 200 μm, Bekaert Co., Ltd.) was employed on the anode side. For the cathode, Pt/C (TEC10E50E, Tanaka Kikinzoku Kogyo K.K.) was mixed with QPAF-4 ionomer (5 wt.% in methanol; IEC = 2.0 meq g^{-1}) and ultrapure water to form the catalyst ink. The ionomer-to-carbon mass ratio was set at 0.6. This ink was deposited onto a Toray TGP-H-120 gas diffusion layer (GDL) using the same PSS system to obtain a gas diffusion electrode (GDE) with a 1.0 cm^2 active area. The cathode catalyst loading was 1.0 mg cm^{-2}. The final MEA was assembled by stacking the CCM, the Ni PTL, and the cathode GDE. EPDM gaskets (200 μm thick on the anode side and 400 μm thick on the cathode side), together with nickel flow-field plates featuring straight channels, were positioned on both sides of the MEA. Gold-plated copper plates served as current collectors. The electrolysis cell was secured by applying a sealing pressure of 0.2 kN at 80 °C for three minutes.

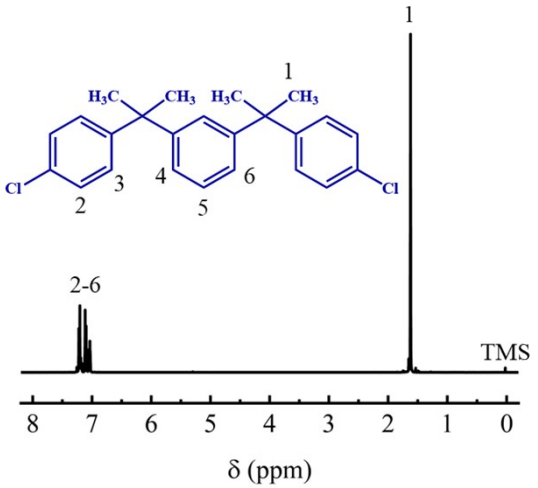

Figure S1. ^{1}H NMR spectrum of 1,3-bis(2-(4-chlorophenyl)propenyl)benzene monomer recorded in $CDCl_3$ at 25 °C.

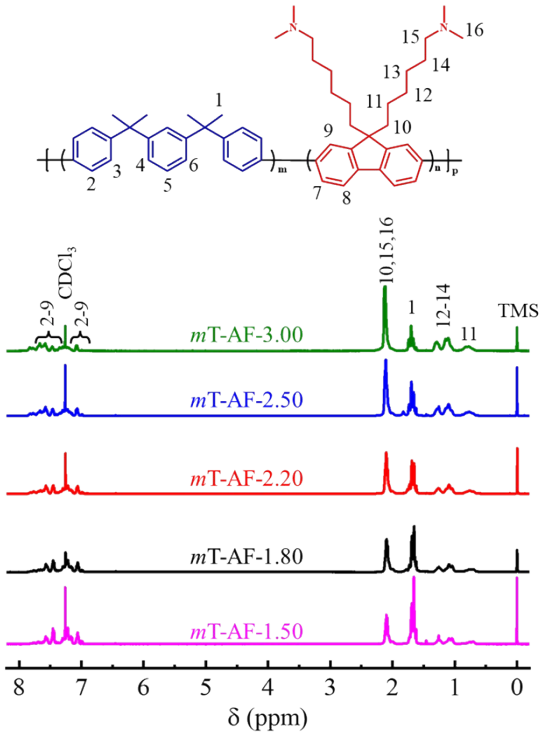

Figure S2. ^{1}H NMR spectra of *m*T-AF-x precursor copolymers recorded in $CDCl_3$ at 25 ^{o}C.

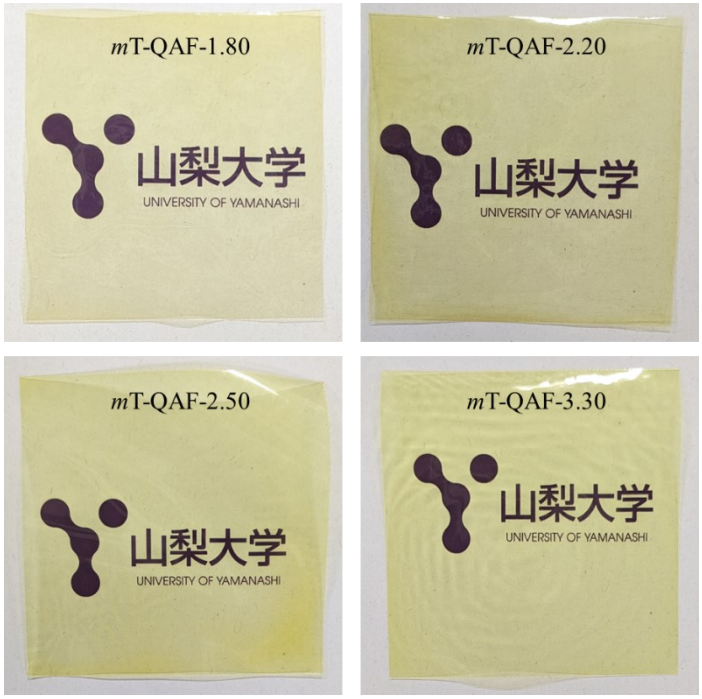

Figure S3. Digital photographs of dry *m*T-QAF-x membranes.

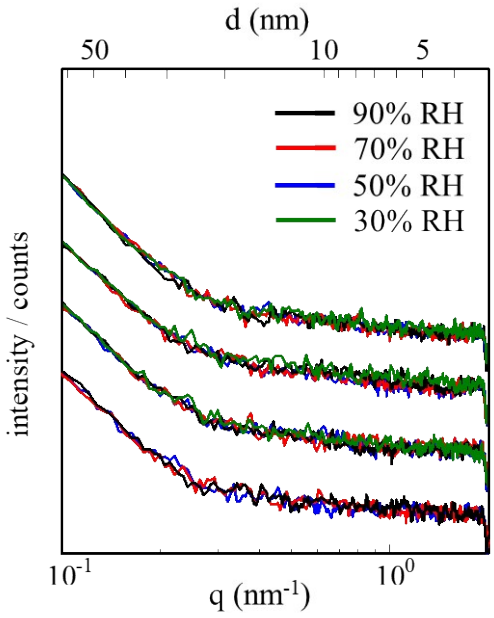

Figure S4. Humidity-dependent SAXS profiles of *m*T-QAF-x membrane samples in Cl^- form recorded at 40 °C.

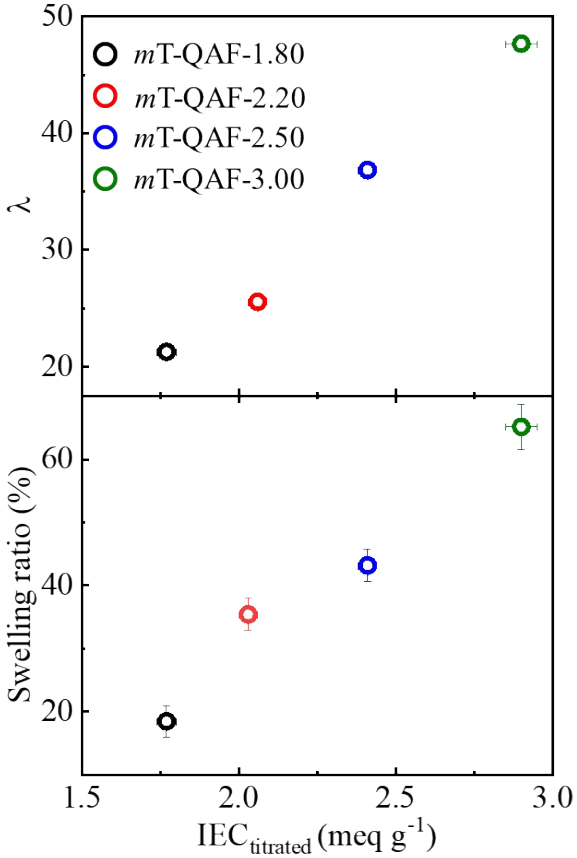

Figure S5. (a) Hydration number (λ) and (b) swelling ratio of *m*T-QAF-x membranes as a function of $IEC_{titrated}$.

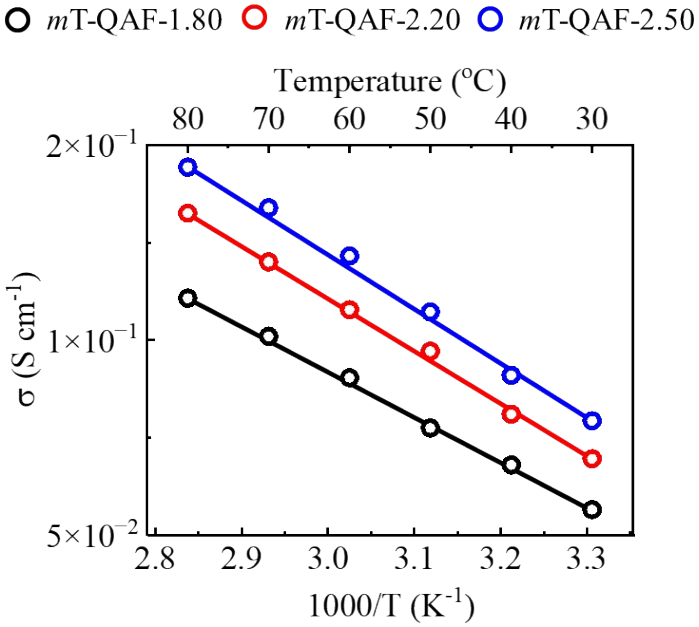

Figure S6. Arrhenius-type temperature dependence of *m*T-QAF-x membranes conductivities in water.

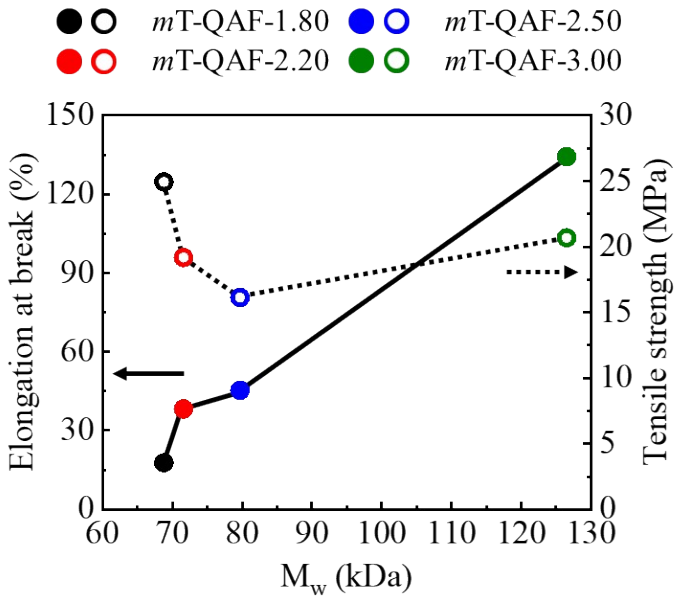

Figure S7. Dependence of elongation at break (solid circles) and tensile strength (open circles) of *m*T-QAF-x membranes on molecular weight (M_w).

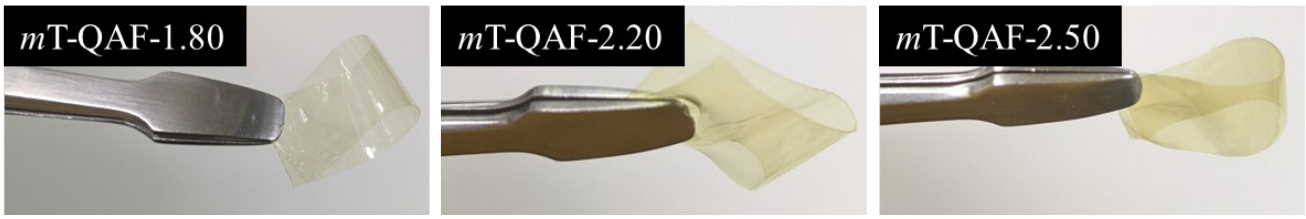

Figure S8. Digital photographs of post-alkaline test (8 M KOH at 80 °C for 1,000 h) membrane samples.

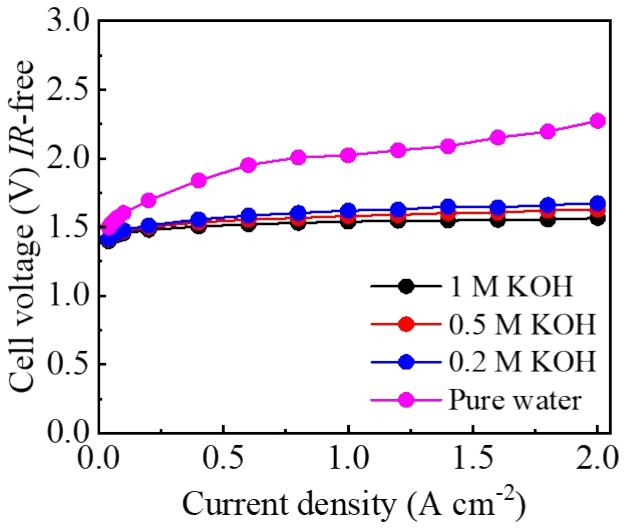

Figure S9. IR-free polarization curve of *m*T-QAF-2.50 AEMWE single cell operated at 80 °C with 1, 0.5, and 0.2 M KOH and pure water feed

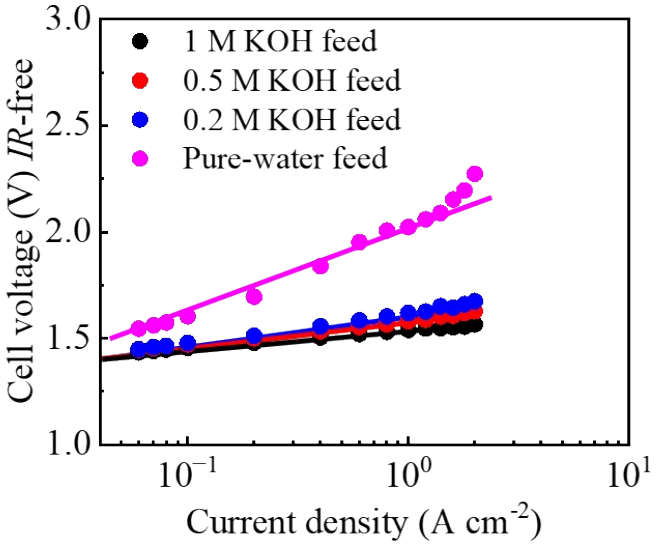

Figure S10. Tafel plots of the *IR*-free cell voltage of the *m*T-QAF-2.50 single cell operated with 1, 0.5, 0.2 M KOH solution, and pure-water feed.

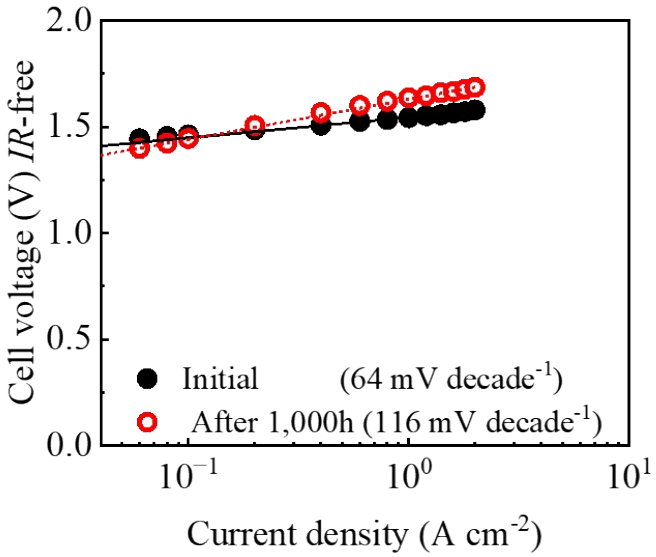

Figure S11. Tafel plots of the *IR*-free cell voltage of the *m*T-QAF-2.50 single cell before and after the *in-situ* durability test.

Table S1. Solubility of *m*T-QAF-x copolymers in various solvents.

Copolymer	DMAc[a]	NMP[a]	MeOH[a]	$CHCl_3$[a]	DMSO[b]
*m*T-QAF-1.50	++	++	--	--	++
*m*T-QAF-1.80	++	++	+-	--	++
*m*T-QAF-2.20	++	++	++	--	++
*m*T-QAF-2.50	++	++	++	--	++
*m*T-QAF-3.00	++	++	++	--	++

[a] Solubility checked at r.t. [b] Solubility checked at 50 °C. ++: Soluble. --: Insoluble. +-: Partially soluble.

Table S2. Comparison of AEMWE performance of this work with reported AEMWEs.

Catalysts		AEM and operating conditions				I-V performance		Reference
Anode	Cathode	AEM	Thickness (μm)	Electrolyte	Temperature (°C)	CD (A cm^{-2})	CP (V)	
$Ni_{0.8}Fe_{0.2}O$	Pt/C	*m*T-QAF-2.50	17	1M KOH	80	1.00	1.58	This work[a]
$Ni_{0.8}Fe_{0.2}O$	Pt/C	*m*T-QAF-2.50	17	1M KOH	80	2.00	1.65	This work[a]
$NiFe^{2+}Fe^{3+}$-LDHs	Pt/C	Versogen A20	NR	1M KOH	80	1.00	1.64	4[b]
$CoCrO_x$	Pt/C	PiperION-A60-HCO3	NR	1M KOH	60	1.50	2.10	5[b]
Ni-Fe	Pt/C	P-B-15	73	1M KOH	80	1.00	1.67	6[a]
NiFe/NF	Pt-HEA-cluster/CeO_2/C	KMem AM01	NR	1M KOH	80	1.00	1.74	7[a]

$NiCo_2O_4$	C-Co-N	LDPE-VBC-TMA	NR	1M KOH	60	1.00	2.33	8[b]
Ni-ferrous layered double hydroxide	Raney Ni	TFC	NR	25Wt.% KOH (	80	1.16	1.80	9[a]
$NiFe_2O_4$	NiFeCo	C-IL-100	50	1M KOH	80	0.55	2.00	10[a]
FeNi LDH/NF	CoP/NF	PTFE/LDH-3	NR	1M KOH	60	1.00	1.80	11[b]
IrO_2	Pt/C	PQP-100	40	1M KOH	85	1.54	2.00	13[a]
$CoFeCe^{0.5}$	Pt/C	X37-50	50	1M KOH	50	1.00	1.66	14[b]
Ni_2Fe_8–Ni_3S_2/NF	Ni_4Mo/MoO_2/NF	X37-50	50	1M KOH	80	1.00	1.65	15[b]
Ni_2P-Fe/NF	Pt/C	PE(VBTAC)	25	1M KOH	80	1.00	1.73	16[c]
$NiMn_2O_4$/KB 70:30	Pt/KB	FAA-3	NR	1M KOH	80	0.53	2.00	17[c]
IrO_2	Pt/C	PBPA	NR	1M KOH	80	1.00	1.68	18[a]
NiFe-LDH	Pt/C	QPTP-IEO$_{15}$	NR	1M KOH	60	1.00	2.35	19[a]
IrO_2/C/CP	Ru_2P/CP	X37-50	50	1M KOH	50	1.00	1.86	20[a]
$Ni_{0.75}Fe_{2.25}O_4$	Pt/C	X37-50	50	1M KOH	42-45	2.00	1.90	21[c]
NiFeV LDH	Pt/C	X37-50	50	1M KOH	50	2.10	1.80	22[b]
NiFe LDH	PtRu/C	HWU-AEM	NR	1M KOH	r.t.	0.91	1.90	23[a]
IrO_2	Pt/C	PFPB-QA	NR	1M KOH	70	1.53	2.00	24[a]
Ir black	Pt/C	HMT-PMBI	NR	1M KOH	60	1.00	1.74	25[a]

Ir black	Pt/C	AF1-HNN8-50	50	1M KOH	60	1.00	1.69	26[a]
IrO_2	PtRu/C	PTP-C1	NR	1M KOH	80	1.00	1.66	27[b]
Ir-Ni/Mo_5N_6	Ir-Ni/Mo_5N_6	X37-50	50	1M KOH	80	2.10	2.00	28[a]
IrO_2	Pt/C	QMter-co-Mpi-100%	NR	1M KOH	50	1.06	2.50	29[a]

CD- current density, CP- cell potential (*IR*-included), NR- not reported

[a] electrolyte supply on both side, [b] not reported, and [c] electrolyte supplied to anode only

Table S3. Durability comparison of *m*T-QAF-2.50 cell with reported AEMWE cells.

Catalyst		AEM and thickness		In-situ durability conditions						Ref.
Anode	Cathode	Name	µm	Electrolyte	Temp. (°C)	CD (A cm^{-2})	EOL (V)	VDR (µV h^{-1})	Time (h)	
$Ni_{0.8}Fe_{0.2}O$	Pt/C	*m*T-QAF-2.50	17	1M KOH	80	1.00	1.68	89	1,000	This work
$CoCrO_x$	Pt/C	PiperION-A60-HCO3	NR	1M KOH	60	0.50	~>2.20	NR	120	5
Ni-Fe	Pt/C	P-B-15	73	1M KOH	80	1.00	1.67	32	500	6
NiFe/NF	Pt-HEA-cluster/CeO_2/C	KMem AM01	NR	1M KOH	r.t.	0.50	~1.76	NR	500	7
$NiCo_2O_4$	C-Co-N	LDPE-VBC-TMA	NR	1M KOH	20	0.50	2.36	NR	96	8
Ni-ferrous layered double hydroxide	Raney Ni	KOH TFC	NR	5 Wt.%	60	0.20	~1.62	50	1,000	9
$NiFe_2O_4$	NiFeCo	C-IL-100	50	1M KOH	50	0.10	1.81	NR	8.3	10

FeNi LDH/NF	CoP/NF	PTFE/LDH-3	NR	1M KOH	60	0.50	1.65	NR	180	11
Co_3O_4 TP-85	Pt/C	PiperION TP-85	NR	0.1M KOH	NR	1.00	~1.75	<1000	18	12
IrO_2	Pt/C	PQP-100	40	1M NaOH	60	0.20	1.89	110	402	13
Ni_2Fe_8–Ni_3S_2/NF	Ni_4Mo/MoO_2/NF	X37-50	50	1M KOH	60	1.00	~1.90	1300	100	15
Ni_2P-Fe/NF	Pt/C	PE(VBTAC)	25	1M KOH	80	0.20	~1.55	NR	24	16
NiFe-LDH	Pt/C	QPTP-IEO_{15}	NR	1M KOH	60	0.20	1.65	NR	18	19
$Ni_{0.75}Fe_{2.25}O_4$	Pt/C	X37-50	50	1M KOH	42-45	0.50	~1.80	NR	21	21
NiFeV LDH	Pt/C	X37-50	50	1M KOH	50	0.50	1.74	NR	100	22
IrO_2	Pt/C	PFPB-QA	NR	1M KOH	70	0.20	~1.69	9.47	5	24
Ir black	Pt/C	HMT-PMBI	NR	1M KOH	60	1.00	1.78	<100	100	25
Ir black	Pt/C	AF1-HNN8-50	50	0.1M KOH	50	0.50	1.76	3210	17	26
IrO_2	PtRu/C	PTP-C1	NR	0.1M KOH	60	1.00	1.95	787	216	27
IrO_2	PtRu/C	PTP-C1	NR	0.1M KOH	60	1.00	2.02	333	300	27
IrO_2	Pt/C	QMter-co-Mpi-100%	NR	1M KOH	50	0.20	2.10	NR	500	29

NR- not reported, CD- cell durability current density, EOL- end of life cell potential, VDR- cell voltage decay rate

References

1. H. Ono, T. Kimura, A. Takano, K. Asazawa, J. Miyake, J. Inukai, K. Miyatake, *J.*

Mater. Chem. A, 2017, **5**, 24804-24812.

2. V. Yadav, K. Miyatake, A. M. A. Mahmoud, F. Liu, F. Xian, L. Guo, C. Y. Wong, T. Iwataki, M. Uchida, K. Kakinuma, *J. Mater. Chem. A*, 2024, **12**, 25429-25441.
3. G. Shi, C. Arata, D. A. Tryk, T. Tano, M. Yamaguchi, A. Iiyama, M. Uchida, K. Iida, S. Watanabe, K. Kakinuma, *ACS Omega*, 2023, **8**, 14, 13068–13077.
4. X. Guo, B. Li, W. Liu, Y. Li, S. Li, Q. Sha, B. Ding, Y. Yang, Y. Zhang, Y. Zhang, H. Xin, L. Bai, D. Zhou, X. Sun, *Adv. Funct. Mater.*, 2025, e1227.
5. S. Li, T. Liu, W. Zhang, M. Wang, H. Zhang, C. Qin, L. Zhang, Y. Chen, S. Jiang, D. Liu, X. Liu, H. Wang, Q. Luo, T. Ding, T. Yao, *Nat. Commun.*, 2024, **15**, 3416.
6. W. Liu, Z. Geng, S. Guo, L. Liu, L. Zhao, C. Qu, Q. Xia, H. Cai, X. Zhao, J. Zhu, J. Chen, L. Jin, C Zhang, *Adv. Energy Mater.*, 2025, **15**, e03110.
7. Wang, H.; Wang, X.; Gao, F.; Chen, J.; Ren, X.; Shen, Z.; Wang, K.; Qi, F.; Liu, Y.; Gao, Y.; Yang, Y.; Wang, D.; Li, Z.; Cui, W.; Pan, H. *Adv. Mater.*, 2025, e14269.
8. S. Radhakrishnan, S. Ramakrishnan, S. K. Jayaraj, M. Mamlouk, B.-S. Kim, *Small*, 2025, **21**, 2411019.
9. J. Choi, H. Kim, S. Jeon, M. G. Shin, J. Y. Seo, Y.-I. Park, H. Park, A. S. Lee, C. Lee, M. J. Kim, H.-S. Cho, J.-H. Lee, *Small*, 2023, **19**, 2300825.
10. X. Wang, R. G. H. Lammertink, *J. Mater. Chem. A*, 2022, **10**, 8401-8412.
11. L. Wan, Z. Xu, B. Wang, *Chem. Eng. J.*, 2021, **426**, 131340.
12. G. A. Lindquist, J.C. Gaitor, W. L. Thompson, V. Brogden, K. J. T. Noonan, S. W. Boettcher, *Energy Environ. Sci.*, 2023, **16**, 4373-4387.
13. M. Liu, X. Hu, B. Hu, L. Liu, N. Li, *J. Membr. Sci.*, 2022, **642**, 119966.
14. Y. S. Park, F. Liu, D. Diercks, D. Braaten, B. Liu, C. Duan, *Applied Catalysis B: Environmental*, 2022, **318**, 121824.

15. G. Ding, H. Lee, Z. Li, J. Du, L. Wang, D. Chen, L. Sun, *Adv. Energy Sustainability Res.*, 2023, **4**, 2200130.
16. S. Sankar, S. Roby, H. Kuroki, S. Miyanishi, T. Tamaki, G. M. Anilkumar, T. Yamaguchi, *ACS Sustainable Chem. Eng.*, 2023, **11**, 854-865.
17. A. Carbone, S. C. Zignani, I. Gatto, S. Trocino, A. S. Aricò, *Int. J. Hydrogen Energy*, 2020, **45**, 9285-9292.
18. Z. Jiang, G. Yi, X. Yao, Y. Ma, X. Su, Q. Liu, Q. Zhang, *Chem. Eng. J.*, 2023, **467**, 143442.
19. X. Cheng, C. Li, X. Zou, B. Sun, L. Wang, W. Wang, X. Meng, *Chem. Eng. J.*, 2024, **483**, 149328.
20. J.-C. Kim, J. Kim, J. C. Park, S. H. Ahn, D.-W. Kim, *Chem. Eng. J.*, 2021, **420**, 130491.
21. J. Lee, H. Jung, Y. S. Park, S. Woo, N. Kwon, Y. Xing, S. H. Oh, S. M. Choi, J. W. Han, B. Lim, *Chem. Eng. J.*, 2021, **420**, 127670.
22. J. Lee, H. Jung, Y. S. Park, S. Woo, J. Yang, M. J. Jang, J. Jeong, N. Kwon, B. Lim, J. W. Han, S. M. Choi, *Small*, 2021, **17**, 2100639.
23. Z. Xu, L. Wan, Y. Liao, P. Wang, K. Liu, B. Wang, *J. Mater. Chem. A*, 2021, **9**, 23485-23496.
24. H. Lim, I. Jeong, J. Choi, G. Shin, J. Kim, T. H. Kim, T. Park, *Applied Surface Science*, 2023, **610**, 155601.
25. B. Chen, P. Mardle, S. Holdcroft, *J. Power Sources*, 2022, **550**, 232134.
26. P. Fortin, T. Khoza, X. Cao, S. Y. Martinsen, A. O. Barnett, S. Holdcroft, *J. Power Sources*, 2020, **451**, 227814.

27. L. Liu, L. Bai, Z. Liu, S. Miao, J. Pan, L. Shen, Y. Shi, N. Li, *J. Membr. Sci.*, 2023, **665**, 121135.

28. H. Wang, Y. Tong, K. Li, P. Chen, *J. Colloid Interface Sci.*, 2022, **628**, 306-314.

29. X. Yan, X. Yang, X. Su, L. Gao, J. Zhao, L. Hu, M. Di, T. Li, X. Ruan, G. He, *J. Power Sources*, 2020, **480**, 228805.